

doi: 10.12029/gc2017Z107

论文引用格式: 曾令森, 高锐, 高利娥, 王海燕, 贺日政, 金胜, 侯贺晟, 薛爱民, 熊小松, 李文辉, 叶高峰. 2017. 中国西部典型盆山结合带: 西秦岭—临夏盆地深地震反射剖面沿线岩浆岩岩石地球化学测试数据集 [J]. 中国地质, 44(S1): 56–63.

数据集引用格式: 曾令森, 高锐, 高利娥, 王海燕, 贺日政, 金胜, 侯贺晟, 薛爱民, 熊小松, 李文辉, 叶高峰. 2017. 中国西部典型盆山结合带: 西秦岭—临夏盆地深地震反射剖面沿线岩浆岩岩石地球化学测试数据集 [DB]. 全球地质数据, DOI: 10.23650/data.G.2017.NGA116411.Z1.1.1.

收稿日期: 2017-06-28

改回日期: 2017-07-28

项目: 国土资源部  
科技创新计划项目  
(1212010711813)资助。

# 中国西部典型盆山结合带: 西秦岭—临夏盆地深地震反射剖面沿线岩浆岩岩石地球化学测试数据集

曾令森 高锐 高利娥 王海燕 贺日政 金胜  
侯贺晟 薛爱民 熊小松 李文辉 叶高峰

(中国地质科学院地质研究所, 北京 100037)

**摘要:** 西秦岭造山带位于青藏高原的东北缘, 其岩石圈结构与变化记录着高原向东北发展演化的深部过程信息。西秦岭造山带也是中国资源开发的远景区, 特别是随着全球石油的紧缺, 我国石油地质界加快了新区勘探, 西秦岭造山带与其两侧盆地被列为中国油气勘探评价值得重视和重新认识的战略选区之一。在野外观测的基础上, 对跨越西秦岭和位于南祁连的临夏盆地的深地震反射剖面沿线的重要地质体进行了系统采样, 开展了锆石 U–Pb 地质年代学、全岩元素和同位素 (Sr 和 Nd) 组成的测试工作。西秦岭—临夏盆地深地震反射剖面沿线重要岩浆岩岩石地球化学测试数据集中共包含 3 个数据表, 分别为合作北部西秦岭造山带和临夏盆地内岩浆岩的锆石 LC–MC–ICP–MS 定年数据 (共计 7 个测试样品、145 个测试点, 测试精度为  $(2\sigma)$  均为 2%)、合作北部西秦岭造山带和临夏盆地内岩浆岩的主量元素和微量元素特征 (共计 33 个测试样品, 每个样品有 69 个测试项, 含量大于  $10 \times 10^{-6}$  的元素的测试精度为 5%, 而小于  $10 \times 10^{-6}$  的元素精度为 10%)、合作北部西秦岭造山带和临夏盆地内岩浆岩的 Sr 和 Nd 同位素特征 (共计 27 个测试样品, Sr 和 Nd 同位素的测试精度分别为  $\pm 0.000010$  ( $n=18$ ), 和  $\pm 0.000011$  ( $n=18$ ))。这些数据为厘定不同岩浆岩的形成年代和地球化学性质, 从而更好地解译地震反射剖面揭示的深部地质构造所代表的构造意义。

**关键词:** 盆山结合带; 西秦岭; 临夏盆地; 地震反射剖面; 岩石地球化学; 数据集

数据服务系统网址: <http://dcc.cgs.gov.cn>

## 1 引言

西秦岭造山带位于青藏高原的东北缘, 其岩石圈结构与变化记录着高原向东北发展演化的深部过程信息。西秦岭造山带又处于中国大陆东西及南北构造交接部位, 特殊的构造环境使其成为研究中国大陆南北汇聚及其与祁连造山带、南北构造带构造转折关系的窗口, 地震活动频繁。中国大陆许多关键时期的构造演化、资源开发及大陆动力学等

第一作者简介: 曾令森, 男, 1970 年生, 博士, 研究员, 岩石与地球化学; E-mail: lzeng1970@163.com。

重大问题，都与西秦岭造山带密切相关。西秦岭造山带也是我国资源开发的远景区，特别是随着全球石油的紧缺，我国石油地质界加快了新区勘探，西秦岭造山带与其两侧盆地被列为中国油气勘探评价值得重视和重新认识的战略选区之一。

合作—永靖地震反射剖面跨越西秦岭和南祁连两条造山带。其中以西秦岭北缘逆冲—走滑断裂为界，南部为西秦岭造山带，北部临夏盆地（图1）。在临夏盆地内部，零星出露钾长花岗岩和基性岩脉，反映了临夏盆地的基底物质组成。该盆地记录了青藏高原隆生过程中的大量构造事件和气候事件而且由于水系的切割，地层出露完好，因而临夏盆地是利用沉积物揭示青藏高原隆升过程的理想场所（李吉均等，1995；方小敏等，1997；郑德文等，2003）。

临夏盆地记录的两次青藏高原隆升的时间，分别为约14 Ma和5.4~8.0 Ma（郑德文等，2003）。其中，约14 Ma的快速剥露事件可能反映青藏高原北部由于岩石圈对流减薄而发生的地壳增厚、高原隆升事件，与区域上钾质碱性火山岩的活动时限相似（喻学惠等，1994，2001）；后一期事件可能与高原隆升到相当高度后，由于维持其巨大高度和继续调节南北汇聚的需要，青藏高原的东北边界向东向北扩展有关（郑德文等，2003）。

地震反射剖面测线（图1中的虚线）跨越西秦岭和位于南祁连的临夏盆地。为更好地解译地震反射剖面揭示的深部地质构造所代表的构造意义，在野外观测的基础上，对合作—永靖地震反射剖面沿线的重要地质体进行了系统采样，开展了锆石U-Pb地质年代学、全岩元素和同位素（Sr和Nd）组成的测试工作，来厘定不同岩浆岩的形成年代和地球化学性质。

西秦岭—临夏盆地深地震反射剖面沿线重要岩浆岩岩石地球化学测试数据集元数据简表如表1所示。

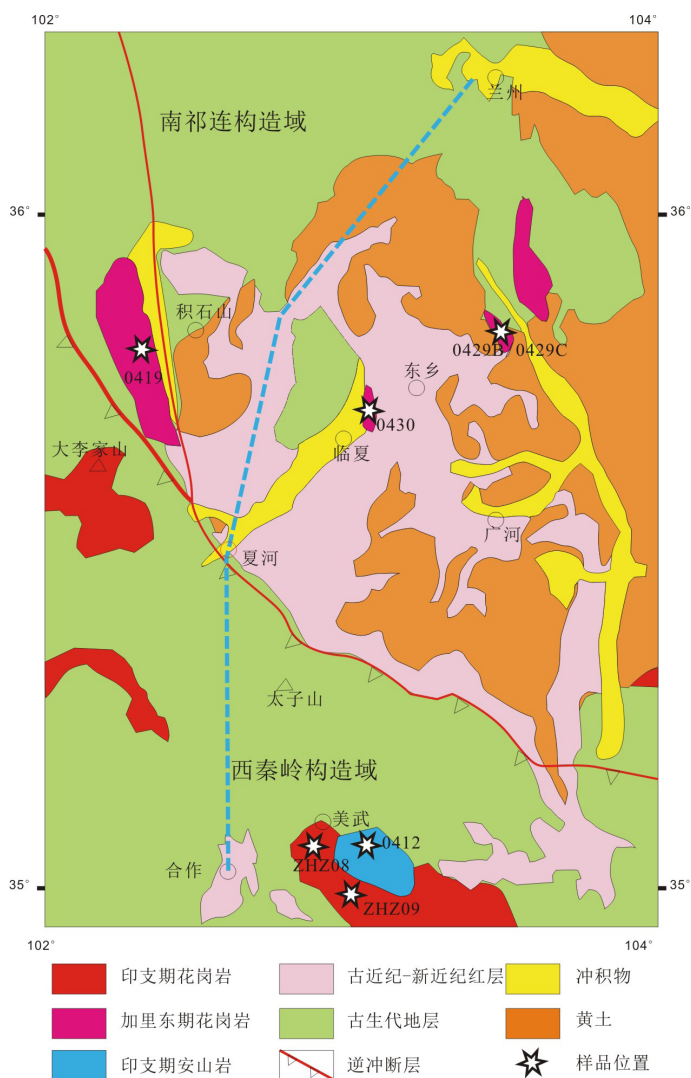


图1 甘肃临夏地区地质简图（据甘肃省区调队，1:20万中华人民共和国地质图临夏幅修篇）

表 1 数据库 (集) 元数据简表

条目	描述
数据库 (集) 名称	中国西部典型盆山结合带：西秦岭—临夏盆地深地震反射剖面沿线岩浆岩岩石地球化学测试数据集
数据作者	曾令森, 中国地质科学院地质研究所 高锐, 中国地质科学院地质研究所 高利娥, 中国地质科学院地质研究所 王海燕, 中国地质科学院地质研究所 贺日政, 中国地质科学院地质研究所 金胜, 中国地质科学院地质研究所 侯贺晟, 中国地质科学院地质研究所 薛爱民, 中国地质科学院地质研究所 熊小松, 中国地质科学院地质研究所 李文辉, 中国地质科学院地质研究所 叶高峰, 中国地质科学院地质研究所
语种	中文
数据时间范围	2007—2010 年
地理区域	甘肃临夏, 东经 102°~104°, 北纬 35°~36°
数据格式	.doc
数据量	150 kB
数据服务系统网址	<a href="http://dcc.cgs.gov.cn">http://dcc.cgs.gov.cn</a>
数据库 (集) 组成	本数据集共有三张数据表组成: (1) 合作北部西秦岭造山带和临夏盆地内岩浆岩的锆石 LC-MC-ICP-MS 定年数据, 命名为: zircon data.xls, 由 7 件样品的锆石 U-Pb 数据组成。(2) 合作北部西秦岭造山带和临夏盆地内岩浆岩的主量元素和微量元素特征, 命名为: major and trace element data.xls, 由 33 件样品的 12 个主量元素含量, 14 个稀土元素含量和 27 个微量元素含量组成。(3) 合作北部西秦岭造山带和临夏盆地内岩浆岩的 Sr 和 Nd 同位素特征, 命名为: Sr and Nd data.xls, 由 27 件样品的 Sr 和 Nd 同位素比值组成。

## 2 区域地质概况

临夏盆地的西北侧为地形较高的积石山, 出露花岗岩和巨晶闪长岩, 其中的花岗岩与临夏盆地内部的类似。临夏盆地位于兰州市西南约 100 km, 是一个以青藏高原东北缘雷积山深大断裂、西秦岭北缘深大断裂, 和马衔山东延余脉围成的具有山前拗陷性质的盆地, 属于古近—新近纪大型陇中盆地的西南隅 (图 1), 盆地开始发育于 30 Ma 年前, 此后新生代地层几乎连续完整至今, 沉积中心古近—新近纪沉积物厚达 1600 m。

## 3 数据采集和处理方法

### 3.1 样品采集

在项目执行过程中, 沿甘肃兰州—合作一线的开展了详细地野外地质调查, 采集了有代表性的岩石样品 (图 2, 图 3), 其中锆石 U-Pb 年代学样品 7 件, 包括花岗岩、钾长花岗岩、花岗闪长岩、闪长岩、英安岩和安山岩。



图2 安山岩 (ZHZ09)侵入到花岗闪长岩 (ZHZ08)

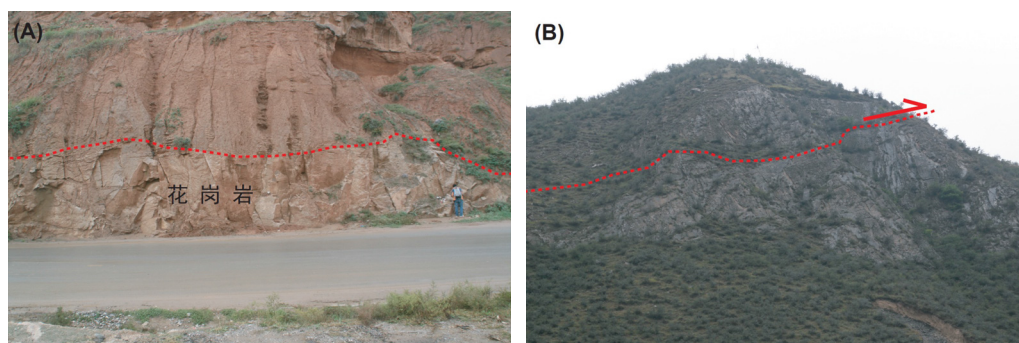


图3 花岗岩 0430 (A)和逆冲断层 (B)的野外照片

## 3.2 样品测试方法及精度

### 3.2.1 锆石 LA-MC-ICP MS 分析方法和锆石特征

选择代表性样品, 粉碎至 60 目, 通过淘洗—磁选—电磁选—手工挑取等一系列方法分离锆石。在双目镜下, 选择干净透明的单矿物颗粒, 逐粒整齐排放于双面胶带上, 按上 PVC 环, 将环氧树脂和固化剂混合均匀后注入 PVC 环, 然后放入烘箱, 60 摄氏度恒温 48 h。取出样品靶, 利用砂纸磨至样品中心部位并用抛光布抛光。靶制备完成后对矿物进行反射光和透射光显微照相, 以查明样品表面的裂隙和内部的包裹体。之后, 在扫描电镜实验室对锆石进行阴极发光图像采集, 检查矿物颗粒的内部结构和成分环带, 以确定合适的位置进行分析测试。在分析测试前, 用酒精超声清洗样品靶, 除去可能的表面污染。采用离子探针方法分析的样品靶需在分析前进行表面镀金。阴极发光成像观察在北京离子探针中心进行, 在中国地质科学院地质研究所, 利用扫描电镜进行了 BSE 图像和锆石内部包裹体的成分测试。通过阴极发光和 BSE 图像来查明锆石内部生长层的分布和结构, 选取测试点。锆石 U-Pb 同位素定年测试在中国地质科学院矿产资源研究所 MC-ICP-MS 实验室完成, 锆石定年分析所用仪器为 Finnigan Neptune 型 MC-ICP-MS 及与之配套的 Newwave UP 213 激光剥蚀系统。激光剥蚀所用斑束直径为  $25\ \mu\text{m}$ , 频率为 10 Hz, 能量密度约为  $2.5\ \text{J}/\text{cm}^2$ , 以 He 为载气。信号较小的  $^{207}\text{Pb}$ ,  $^{206}\text{Pb}$ ,  $^{204}\text{Pb}(+^{204}\text{Hg})$ ,  $^{202}\text{Hg}$  用离子计数器 (multi-ion-counters) 接收,  $^{208}\text{Pb}$ ,  $^{232}\text{Th}$ ,  $^{238}\text{U}$  信号用法拉第杯接收, 实现了所有目标同位素信号的同时接收并且不同质量数的峰基本上都是平坦的, 进而可以获得高精度的数据, 均匀锆石颗粒  $^{207}\text{Pb}/^{206}\text{Pb}$ ,  $^{206}\text{Pb}/^{238}\text{U}$ ,  $^{207}\text{Pb}/^{235}\text{U}$  的测试精度 (2) 均为 2% 左右, 对锆石标准的定年精度和准确度在 1%(2) 左右。LA-MC-ICP-

MS 激光剥蚀采样采用单点剥蚀的方式，数据分析前用锆石 GJ-1 进行调试仪器，使之达到最优状态，锆石 U-Pb 定年以锆石 GJ-1 为外标，U、Th 含量以锆石 M127(U:923×10<sup>-6</sup>; Th:439×10<sup>-6</sup>; Th/U: 0.475. Nasdala et al, 2008) 为外标进行校正。测试过程中在每测定 5~7 个样品前后重复测定两个锆石 GJ1 对样品进行校正，并测量一个锆石 Plesovice，观察仪器的状态以保证测试的精确度。数据处理采用 ICPMSDataCal 程序 (Liu et al. 2010)，测量过程中绝大多数分析点 <sup>206</sup>Pb/<sup>204</sup>Pb>1000，未进行普通铅校正，<sup>204</sup>Pb 由离子计数器检测，<sup>204</sup>Pb 含量异常高的分析点可能受包体等普通 Pb 的影响，对 <sup>204</sup>Pb 含量异常高的分析点在计算时剔除，锆石年龄谐和图用 Isoplot 3.0 程序获得。完成了 7 件锆石 U/Pb 地质年代学测试。

样品 0412 为英安岩，采自于西秦岭造山带内，锆石呈自形、长柱状，棱角清晰，粒度在 100~250 μm，长宽比一般为 2:1，个别可达 3:1。锆石阴极发光和背散射图像都显示锆石没有核部，较干净，基本上不含包裹体，具明显的韵律环带结构 (图 4a)，核部环带密度小，而边部环带密度大，为岩浆锆石。

ZHZ08 为花岗闪长岩，采自于西秦岭造山带内。锆石呈自形、柱状，棱角清晰，粒

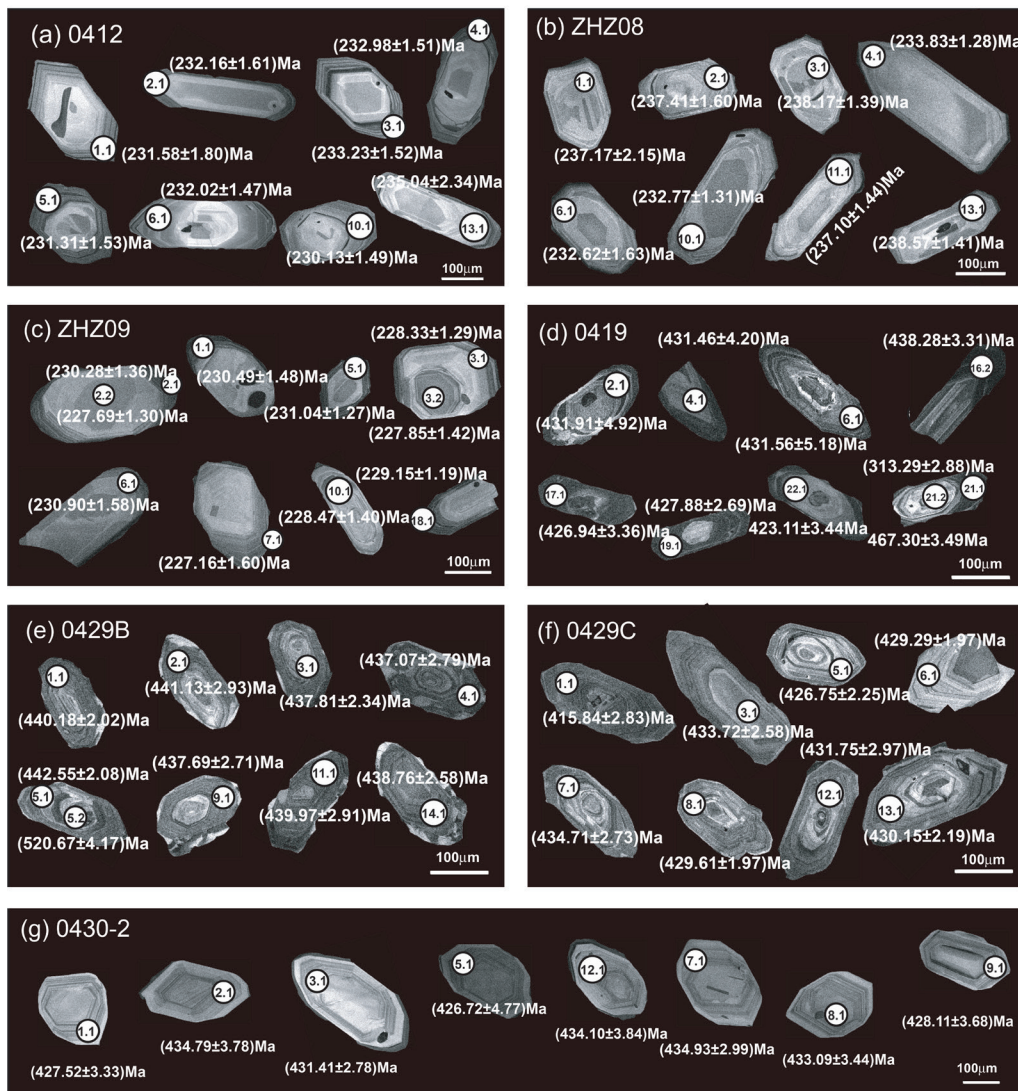


图 4 岩石样品代表性锆石阴极发光照片

度在 100~250  $\mu\text{m}$ ，长宽比一般为 2 : 1~3 : 1。锆石阴极发光和背散射图像都显示锆石没有核部，较干净，个别含包裹体，具弱化的韵律环带结构（图 4b），为岩浆锆石，但可能受到后期热事件的影响。

ZHZ09 为安山岩，采自于西秦岭造山带内，锆石呈自形一半自形，大部分为长柱状，个别为浑圆状，粒度在 50~200  $\mu\text{m}$ ，长宽比一般为 2 : 1~3 : 1。锆石阴极发光和背散射图像都显示锆石没有核部，较干净，个别含包裹体，具弱化的韵律环带结构（图 4c），个别锆石边部由于含有较高的 U 和 Th，显示暗色发光的韵律环带，但是与核部锆石为同一期，可能是由于同期事件中锆石生长时 U、Th 变化引起的。

0419 为钾长花岗岩，采自于积石山。锆石呈自形一半自形，长柱状，粒度在 100~200  $\mu\text{m}$ ，长宽比一般为 2 : 1，个别达 4 : 1。锆石阴极发光和背散射图像都显示锆石具有核-幔-边结构，白色模糊环带的核部，灰色弱环带的幔部和黑色弱发光的边部，个别锆石的幔部含有包裹体（图 4d）。

0429B 为闪长岩，采自于临夏盆地的北侧的唐旺镇。锆石呈半自形—他形，柱状、浑圆状，粒度在 50~150  $\mu\text{m}$ ，大部分长宽比为 2 : 1，少量为 1 : 1。锆石阴极发光和背散射图像都显示锆石具有核-幔-边结构，弱振荡环带的核部，灰色无环带的幔部和白色的窄边（图 4e）。

0429C 为钾长花岗岩，采自于临夏盆地的北侧的唐旺镇。锆石呈自形，长柱状，粒度为 100~150  $\mu\text{m}$ ，长宽比一般为 2 : 1。锆石阴极发光和背散射图像都显示锆石具有核-边结构，白色含有包裹体的核部，明显的振荡环带的边部（图 4f）。

0430-2 为花岗岩，采自于临夏市北 3 km 处。锆石呈自形，柱状，粒度在 150~200  $\mu\text{m}$ ，长宽比为 2 : 1。锆石阴极发光和背散射图像都显示锆石显示均一的明显振荡环带（图 4g）。

### 3.2.2 主量元素、微量元素分析方法

为确定岩石的地球化学特征，分析了岩石的全岩主量、微量元素和 Rb-Sr、Sm-Nd 同位素组成。主量及微量元素的测试在国土资源部国家地质实验测试中心进行。全岩主量元素采用 X 荧光光谱 (XRF) 玻璃熔片法进行分析。流程如下：首先将全岩粉末在 105  $^{\circ}\text{C}$  的烘箱中烘烤 2 h，去除样品中的吸附水。将样品从烘箱中取出后迅速放入干燥器中冷却。待样品冷却至室温后，准确称取 0.5 g ( $0.5000 \pm 0.0007\text{g}$ ) 样品放入已恒重的坩埚中，之后将盛有样品的坩埚放入马弗炉中加热至 1000  $^{\circ}\text{C}$  灼烧 1.5 h。取出灼烧后的样品置于干燥器中，冷却至室温后称重，计算样品的烧失量。之后，准确称取混合试剂（成分为溶剂  $\text{Li}_2\text{B}_4\text{O}_7$ 、助溶剂 LiF、氧化剂  $\text{NH}_4\text{NO}_3$ ）5 g，与样品混合并研磨至均匀。将混合样品倒入铂金坩埚中，加入 3 滴溴化锂（脱模剂），在高频熔样机内 1000  $^{\circ}\text{C}$  下充分熔融后倒出，冷却形成玻璃熔片。最后，利用 XRF (X 荧光光谱仪 3080E) 对样品进行主量元素分析。在分析过程中，选用国家标准物质中心提供的岩石标样 GSR.1（花岗岩）、GSR.2（安山岩），GSR.3（玄武岩）作为标准参考物质。分析结果中，分析精度为 5%。

全岩微量元素的分析采用混合酸溶法溶样。分析测试采用离子质谱仪 (ICP-MS-Excell) 完成。分析流程如下：首先将样品放入烘箱内在 105  $^{\circ}\text{C}$  下烘烤 2 h，除去吸附水。将样品取出后置于干燥器中冷却至室温。准确称量 50.00 mg (49.00~51.00 mg) 样品放入 Teflon 有盖溶样弹中，并加入 1.5 mL 高纯  $\text{HNO}_3$ 、1.5 mL 高纯 HF 和 0.01 mL 高纯

HClO<sub>4</sub>。将盛有样品的溶样弹置于 140 °C 的电热板上开盖蒸干，以除去大部分 SiO<sub>2</sub>。蒸干后，再向溶样弹中加入 1.5 mL 高纯 HNO<sub>3</sub>、1.5 mL 高纯 HF。随后将溶样弹加盖并装入钢套密封，放入烘箱中 190 °C 恒温 120 h。取出溶样弹，蒸干样品，然后加入 3 mL 高纯 HNO<sub>3</sub> 再次蒸干，以去除残余的 HF。之后，加入 3 mL 1:1 高纯 HNO<sub>3</sub>，放入钢套中置于烘箱中 150 °C 恒温 12 h，以保证完全提取样品。冷却后，将样品倒入 100 mL PET 瓶中，并加入 1 g Rh 内标，加水定容至 100 g，待上机测试。微量元素和稀土元素 (REE) 含量大于 10×10<sup>-6</sup> 的元素的测试精度为 5%，而小于 10×10<sup>-6</sup> 的元素精度为 10%。个别在样品中含量低的元素，测试误差大于 10%。

### 3.2.3 全岩 Sr-Nd-Pb 同位素分析方法

Rb-Sr 和 Sm-Nd 同位素分析在中国地质科学院地质研究所同位素实验室进行。首先称取 100~150 mg 样品放入 Teflon 有盖溶样弹中，加入 1.5 mL 高纯 HNO<sub>3</sub>，1.5 mL 高纯 HF 和 0.01 mL 高纯 HClO<sub>4</sub>，放在 140 °C 的电热板上开盖加热蒸干。蒸干后加入 1 mL 高纯 HNO<sub>3</sub>，2 mL 高纯 HF，加盖装入钢套中，放入烘箱中 190 °C 温度下加热 120 h。取出样品后置于 140 °C 电热板上蒸干。加入 1 mL 6N HCl，再次蒸干并升温至 200 °C 直至白烟冒净。加入 1 mL 3N HCl，保持 80 °C 温度下静置保温过夜，待化学分离。通过同位素稀释法，利用 Finnigan MAT-262 质谱仪测试 Sr 同位素组成及 Rb、Sr、Sm 和 Nd 的浓度。利用 Nu Plasam HR MC-ICP-MS 多接收等离子质谱仪 (Nu Instruments) 进行 Nd 同位素分析。Nd 和 Sr 分析结果通过分别标准化到 <sup>146</sup>Nd/<sup>142</sup>Nd = 0.7219 和 <sup>86</sup>Sr/<sup>88</sup>Sr = 0.1194 进行质量分馏校正。在分析样品期间，Sr 同位素测试标准为 NBS987，测试值为 0.710247±12 (2σ)。Nd 同位素标准为 JMC Nd，测试值为 0.511127±12 (2σ)。Sr 和 Nd 同位素的测试精度分别为 ±0.000010 (n=18)，和 ±0.000011 (n=18)。

## 4 数据样本描述

以 0412 英安岩测试数据为例，说明本数据集的组成和结构。

合作北部西秦岭造山带和临夏盆地内岩浆岩的锆石 LC-MC-ICP-MS 定年数据表中记录了岩浆岩样品的锆石 U-Pb 年龄。“Pb”、“Th”、“U”为测试点的三个元素的含量，单位 μg/g；“Th/U”为两个元素含量比值；“<sup>207</sup>Pb/<sup>206</sup>Pb(Ratio)”、“<sup>207</sup>Pb/<sup>206</sup>Pb(±%)”、“<sup>207</sup>Pb/<sup>235</sup>U(Ratio)”、“<sup>207</sup>Pb/<sup>235</sup>U(±%)”、“<sup>206</sup>Pb/<sup>238</sup>U(Ratio)”、“<sup>206</sup>Pb/<sup>238</sup>U(±%)”分别为各同位素比值及其误差；“<sup>207</sup>Pb/<sup>206</sup>Pb Age(Ma)”、“<sup>206</sup>Pb/<sup>238</sup>U Age(Ma)”、“Concordance”分别为计算获得的年龄值及误差，确定样品的锆石年龄时，使用 “<sup>206</sup>Pb/<sup>238</sup>U(Ma)” 值。以上数据均由实验室测定或计算提供。

合作北部西秦岭造山带和临夏盆地内岩浆岩的主量元素和微量元素特征表中，各主量元素 (单位: wt.%) 和微量元素 (10<sup>-6</sup>) 的含量由实验室测定；“Total”、“FeO<sup>#</sup>”、“Mg<sup>#</sup>”、“A/CNK”、“ΣREE”、“Eu/Eu\*”、“Ce/Ce\*”、“(La/Yb)<sub>N</sub>”、“(La/Gd)<sub>N</sub>”、“(Gd/Yb)<sub>N</sub>” (标准化值据 Sun and McDonough, 1989)、“Nb/Ta”、“Zr/Y”、“Zr/Hf”、“Rb/Sr”、“Rb/Cs” 计算所得。

合作北部西秦岭造山带和临夏盆地内岩浆岩的 Sr 和 Nd 同位素特征表中，“Rb(10<sup>-6</sup>)”、“Sr(10<sup>-6</sup>)”、“<sup>87</sup>Rb/<sup>86</sup>Sr”、“<sup>87</sup>Sr/<sup>86</sup>Sr”、“±2σ” 分别为 Rb、Sr 的含量及同位素比值和误差，由实验室测定提供；“Sm(10<sup>-6</sup>)”、“Nd(10<sup>-6</sup>)”、“<sup>147</sup>Sm/<sup>144</sup>Nd”、“<sup>143</sup>Nd/<sup>144</sup>Nd”、“±2σ” 分

别为该样品的 Sm、Nd 含量及同位素比值和误差，由实验室测定提供；“(87Sr/86Sr)<sub>i</sub>”为计算获得的岩石样品的初始同位素比值，“ $\epsilon_{Nd(i)}$ ”计算获得。

## 5 数据使用方法

以上数据测试结果均为实验室提供。锆石 U-Pb 年龄数据可使用 Isoplot 3.0 程序获得锆石年龄谐和图。主量元素、微量元素和岩石 Sr-Nd 测试数据可分别进行地球化学投图，从而获得岩石地球化学特征，进而推测所采岩石样品的形成机制及研究区的构造背景。

## 6 结论

西秦岭—临夏盆地深地震反射剖面沿线重要岩浆岩岩石地球化学测试数据集中共包含三个数据表，分别为合作北部西秦岭造山带和临夏盆地内岩浆岩的锆石 LA-MC-ICP-MS 定年数据（共计 7 个测试样品、145 个测试点）、合作北部西秦岭造山带和临夏盆地内岩浆岩的主量元素和微量元素特征（共计 33 个测试样品，每个样品有 69 个测试项）、合作北部西秦岭造山带和临夏盆地内岩浆岩的 Sr 和 Nd 同位素特征（共计 27 个测试样品）。这些数据为研究该区域岩石成因和地质构造背景提供了科学数据参考。

## 参考文献

- 方小敏, 李吉均, 朱俊杰, 陈怀录, 曹继秀. 1997. 甘肃临夏盆地新生代地层绝对年代测定与划分 [J]. 科学通报, 42(14): 1457-1471.
- 甘肃省区调队. 1965. 1:20 万中华人民共和国地质图说明书（临夏幅）[M]. 北京：地质出版社.
- 李吉钧, 方小敏, 朱俊杰. 1995. 临夏盆地新生代地层古地磁年代与模式序列 [C]// 青藏高原形成演化、环境变迁与生态系统研究学术论文年刊 (1994). 北京：科学出版社, 41-54.
- Sun S S, McDonough W F. 1989. Chemical and Isotopic Systematics of Oceanic Basalts: Implications for Mantle Composition and Processes [M]. Geological Society, London, Special Publications, 42: 313-34.
- 喻学惠. 1994. 甘肃礼县—宕昌地区新生代钾质碱性超基性火山岩的特征及成因 [J]. 特提斯地质, 18: 114-129.
- 喻学惠, 莫宣学, Martin F, 苏尚国, 赵欣. 2001. 甘肃西秦岭新生代钾霞橄黄长岩火山作用及其构造含义 [J]. 岩石学报, 17(3): 366-377.
- 郑德文, 张培震, 万景林, 李传友, 曹继秀. 2003. 青藏高原东北边缘晚新生代构造变形的时序——临夏盆地碎屑颗粒磷灰石裂变径迹记录 [J]. 中国科学 (D 辑), 33(增刊): 190-198.

(责任编辑 李亚萍 贾丽琼)

Received: 28-06-2017  
Accepted: 28-07-2017

Fund support: Supported  
by Department of  
Land and Resources  
science and technology  
innovation program  
(1212010711813).

doi: 10.12029/gc2017Z107

Article Citation: Zeng Lingsen, Gao Rui, Gao Li'e, Wang Haiyan, He Rizheng, Jin Sheng, Hou Hesheng, Xue Aimin, Xiong Xiaosong, Li Wenhui, Ye Gaofeng. 2017. Geochemical dataset of magmatic rocks along the deep seismic reflection profile of a typical basin-range junction belt in western China: the western Qinling—Linxia Basin [J]. *Geology in China*, 44(S1): 69–78.

Dataset Citation: Zeng Lingsen, Gao Rui, Gao Li'e, Wang Haiyan, He Rizheng, Jin Sheng, Hou Hesheng, Xue Aimin, Xiong Xiaosong, Li Wenhui, Ye Gaofeng. 2017. Geochemical dataset of magmatic rocks along the deep seismic reflection profile of a typical basin-range junction belt in western China: the western Qinling—Linxia Basin [DB]. *Global Geology Data*, DOI: 10.23650/data.G.2017.NGA116411.Z1.1.1

## Geochemical Dataset of Magmatic Rocks along the Deep Seismic Reflection Profile of a Typical Basin-range Junction Belt in Western China: the Western Qinling—Linxia Basin

ZENG Lingsen, GAO Rui, GAO Li'e, WANG Haiyan, HE Rizheng, JIN Sheng, HOU Hesheng, XUE Aimin, XIONG Xiaosong, LI Wenhui, YE Gaofeng

(*Institute of Geology, Chinese Academy of Geological sciences, Beijing 100037, China*)

**Abstract:** The western Qinling orogenic belt is located in the northeastern margin of the Qinghai-Tibet Plateau, and its lithosphere structure and changes record the deep process information of the plateau to the northeast. The western Qinling orogenic belt is also a prospect for resource development in China. Especially because of the shortage of global oil, China's petroleum geology has accelerated the exploration in new areas. The western Qinling orogenic belt and both its basins are listed as one of the most worthy of oil and gas exploration strategic constituencies. On the basis of field observation, important geological bodies along the deep seismic reflection profiles across the West Qinling Mountains and the Linxia basin in southern Qilian were sampled. Zircon U–Pb geology chronology, whole rock elements and isotope (Sr and Nd) composition of the test work resulted in a dataset containing three data tables, including the zircons LA–MC–ICP–MS of magmatic rocks from the western Qinling orogenic belt and the Linxia basin (a total of 7 test samples, 145 test points, the test accuracy of ( $2\sigma$ ) are 2%), major and trace elements of investigated magmatic rocks (a total of 33 test samples, each sample with 69 test items, the content of more than  $10 \times 10^{-6}$  elements with test accuracy of 5%, and less than  $10 \times 10^{-6}$  element accuracy of 10%), and whole-rock Sr and Nd isotopic data for magmatic rocks ( $Sr \pm 0.000010$  ( $n = 18$ ) and  $Nd \pm 0.000011$  ( $n = 18$ ), respectively, in 27 test samples from the western Qinling orogenic belt and the Linxia basin). These data are used to determine the ages and geochemical properties of different magmatic rocks, in order to better explain the tectonic significance represented by the deep geological structure revealed by the seismic reflection profile.

**Key words:** basin–range junction belt; west Qinling—Linxia basin; seismic reflection; litho-geochemistry; dataset

**Data service system URL:** <http://dcc.cgs.gov.cn>

### 1 Introduction

Western Qinling orogenic belt is located in the northeastern margin of the Tibetan Plateau, and its lithosphere structure and record of change can show information on the

**About the first author:** ZENG Lingsen, male, born in 1970, doctor, researcher, majors in rocks and geochemistry; E-mail: lzeng1970@163.com.

deep processes of the northeastward development and evolution of the plateau. The western Qinling orogenic belt is also located in the east-west and south-north tectonic junction of the Chinese continent, and this special tectonic environment makes it the best region for studying the convergence of the north and south terranes/plates of the Chinese continent and their tectonic transition relationship with the Qilian orogenic belt and the north-south tectonic zone. Seismic activities are frequent in this region. Many major aspects such as tectonic evolution, resource exploitation and continental dynamics in many crucial periods of the Chinese continent are closely related to the western Qinling orogenic belt, which therefore is also a prospect area for China's resource exploitation. Especially with the global oil shortage, China's petroleum geoscience industry has speeded up exploration in such new areas. The western Qinling orogenic belt and basins on both its sides have been listed as one of the strategic target areas that deserve focus and re-understanding for oil and gas exploration in China.

The Hezuo—Yongjing seismic reflection profile crosses both the western Qinling and southern Qilian orogenic belts. In this profile, with a thrust-strike slip fault in the northern margin of the western Qinling as a boundary, the western Qinling orogenic belt is to the south, and the Linxia basin to the north located in southern Qilian (Fig. 1). In the Linxia basin, there are sporadic k-feldspar granites and mafic dikes outcropping, reflecting the basement material composition of the basin. The basin also records a large number of tectonic and climatic events during the uplift process of the Tibetan Plateau, and stratum outcrops are intact due to the cutting of the water system. Therefore, the Linxia basin is a satisfactory place to reveal the uplift process of the Tibetan Plateau through its sediments (Li et al., 1995; Fang et al., 1997; Zheng et al., 2003).

The two Tibetan Plateau uplift periods recorded in the Linxia basin were about 14 Ma and about 5.4–8.0 Ma, respectively (Zheng et al., 2003). The rapid denudation event that occurred in about 14 Ma may reflect contemporaneous crustal thickening and plateau uplift events, which happened in the northern part of the Tibetan Plateau due to the convective thinning of the lithosphere; the duration of this activity is similar to that of the potassium alkaline volcanic rocks in the area (Yu et al., 1994, 2001). The latter event may have been associated with the eastward and northward expansion of the northeast boundary of the Tibetan Plateau after the uplift of the plateau reached a considerable height, due to the need to maintain its great height and to continue to regulate the convergence of the north and south (Zheng et al., 2003).

The seismic reflection (SR) profile survey line (dotted line in Fig. 1) crossed the western Qinling and the Linxia basin. In order to better interpret the tectonic meaning of the deep geological structure revealed by the SR profile, on the basis of field observation, systematic sampling of important geological bodies along the Hezuo—Yongjing SR profile was carried out, and analysis of zircon U–Pb geochronology, whole rock elements and isotope (Sr and Nd) composition was conducted, in order to determine the formation age and geochemical characteristics of different magmatic rocks.

The brief table of metadata of the geochemical dataset of important magmatic rocks along the deep SR profile of the western Qinling—Linxia basin is shown in Table 1.

## 2 Overview of regional geology

On the northwest side of the Linxia basin, Jishishan Hill has high terrain and outcropping

**Table 1 Metadata table of dataset(s)**

Items	Description
Database (dataset) name	Geochemical Dataset of Magmatic Rocks along the Deep Seismic Reflection Profile of a Typical Basin-range Junction Belt in Western China: the Western Qinling—Linxia basin
Database authors	Zeng Lingsen, Institute of Geology, Chinese Academy of Geological sciences Gao Rui, Institute of Geology, Chinese Academy of Geological sciences Gao Li'e, Institute of Geology, Chinese Academy of Geological sciences Wang Haiyan, Institute of Geology, Chinese Academy of Geological sciences He Rizheng, Institute of Geology, Chinese Academy of Geological sciences Jin Sheng, Institute of Geology, Chinese Academy of Geological sciences Hou Hesheng, Institute of Geology, Chinese Academy of Geological sciences Xue Aimin, Institute of Geology, Chinese Academy of Geological sciences Xiong Xiaosong, Institute of Geology, Chinese Academy of Geological sciences Li Wenhui, Institute of Geology, Chinese Academy of Geological sciences Ye Gaofeng, Institute of Geology, Chinese Academy of Geological sciences
Language	Chinese
Data acquisition time	From 2007 to 2010
Geographic area	Linxia, Gansu province, east longitude 102°~104°, latitude 35°~36°
Data format	.doc
Data size	150 kB
Data service system URL	<a href="http://dcc.cgs.gov.cn">http://dcc.cgs.gov.cn</a>
Database (set) composition	This dataset comprises three data sheets: (1) The Zircon LC–MC–ICP–MS age data of magmatic rocks in the western Qinling orogenic belt and Linxia basin in the north part of Hezuo, named as: zircon data.xls, consisting of the zircon U–Pb data of 7 samples. (2) The characteristics of major elements and trace elements of magmatic rocks in the western Qinling orogenic belt and Linxia basin in the north part of Hezuo, named as: major and trace element data.xls, consisting of the contents of 12 major elements, 14 rare earth elements and 27 trace elements of 33 samples. (3) The characteristics of Sr and Nd isotopes of magmatic rocks in the western Qinling orogenic belt and Linxia basin in the north part of Hezuo, named as: Sr and Nd data.xls, consisting of Sr and Nd isotope ratios of 27 samples.

granite and megacryst diorite, with the granite similar to that in the Linxia basin. Linxia basin is located about 100 km to the southwest of Lanzhou city. It is a basin with piedmont depression characteristics surrounded by the Leijishan deep fault in the northeastern margin of the Tibetan Plateau, the deep fault in the northern margin of the western Qinling, and the eastward extension of Maxianshan Hill. It belongs to the southwest corner of the large Tertiary Longzhong basin (Fig. 1), which began to develop around 30 Ma, after which, the Cenozoic strata have been almost continuous and kept intact till now. The thickness of the Tertiary sediments in the depocenter is up to 1600 m.

### 3 Data acquisition and processing methods

#### 3.1 Sample collection

During the implementation of the project, a detailed field geological survey was

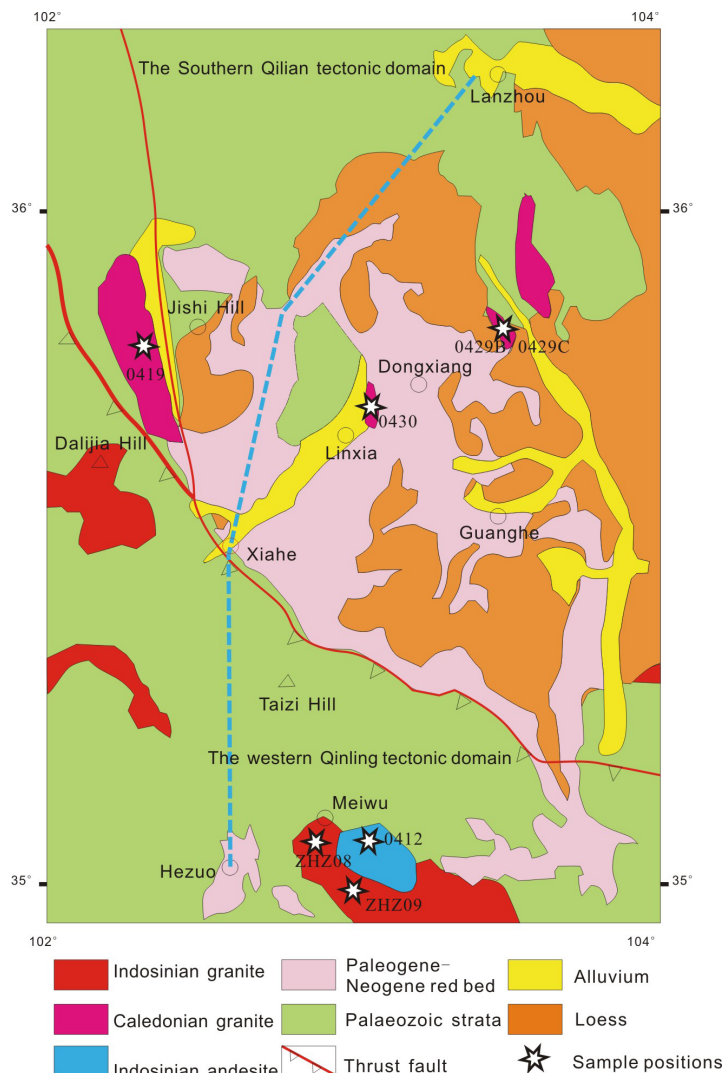


Fig. 1 Geological map of Linxia, Gansu Province (after the Geological Survey of Gansu Province)

conducted along the Gansu Lanzhou—Hezuo line, and representative rock samples were collected (Fig. 2 and Fig. 3), of which 7 pieces are zircon U–Pb geochronology samples, including granite, K–feldspar granite, granodiorite, diorite, quartz andesite, and andesite.

## 3.2 Sample analytical procedures and accuracy

### 3.2.1 Zircon LA–MC–ICP–MS analysis method and zircon characteristics

A representative sample was selected, crushed into 60 mesh, and the zircon separated by a series of methods, namely washing, magnetic separation, electromagnetic separation, and manual separation. Under a binocular microscope, clean and transparent single-mineral particles were selected, and placed one by one on double-sided tape, and then a PVC ring pressed on. After mixing epoxy resin and its curing agent evenly, the mixture is poured into the PVC ring, and then placed into an oven, and kept at 60°C for 48 hours. Taking out the sample target, it was sanded with a piece of sandpaper to the central portion and polished with a piece of polishing cloth. After the target preparation was completed, reflected and transmitted light photomicrography was conducted on the mineral to identify



Fig. 2 Field photographs showing the andesite ZHZ09 intruding into granodiorite ZHZ08

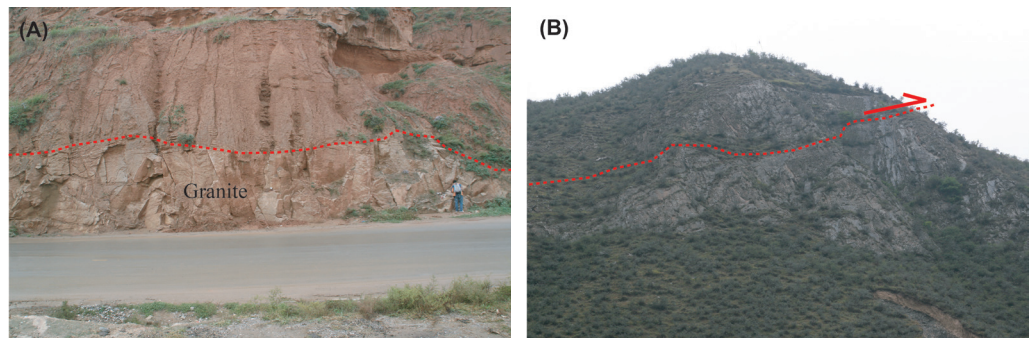


Fig. 3 Field photographs showing the granite 0430 (A) and thrust fault (B)

surface cracks and internal inclusions of the sample. Thereafter, cathodoluminescence (CL) image acquisition was conducted for the zircon in the scanning electron microscope laboratory to examine the internal structure and composition zoning of mineral particles, to determine the appropriate position for analysis and testing. Prior to the analysis and testing, the sample target was cleaned ultrasonically with alcohol, to remove possible surface contamination. The sample target was plated with gold on the surface and then was analyzed using the ion probe method. The CL imaging observation was carried out at the Beijing SHRIMP Center, and the backscattered (BSE) imaging and the test of components of inclusions in zircon were conducted using scanning electron microscopy at the Institute of Geology, Chinese Academy of Geological Sciences, Beijing. The distribution and structure of the growth layer in zircon were determined by CL and BSE images, to select analysis points. The zircon U–Pb analyses were conducted in the MC-ICP-MS laboratory of the Institute of Mineral Resources, Chinese Academy of Geological Sciences. The equipment used for the zircon dating analysis is the Finnigan Neptune MC - ICP - MS and its accompanying Newwave UP 213 Laser Ablation system. In laser ablation, the diameter of the beam spot used is 25  $\mu\text{m}$ , the frequency is 10 Hz, the energy density is about 2.5 J/cm<sup>2</sup>, and the carrier gas is He. Multi-ion-counters were used to receive signals for <sup>207</sup>Pb, <sup>206</sup>Pb, <sup>204</sup>Pb(+<sup>204</sup>Hg) and <sup>202</sup>Hg with weak signals, and the signals of <sup>208</sup>Pb, <sup>232</sup>Th, and <sup>238</sup>U were received using Faraday cups; therefore, all target isotope signals were simultaneously received and all peaks with different mass numbers were substantially planar, to obtain data with high accuracy. The test accuracies (2s) of <sup>207</sup>Pb/<sup>206</sup>Pb, <sup>206</sup>Pb/<sup>238</sup>U and <sup>207</sup>Pb/<sup>235</sup>U of uniform zircon particles are all about 2%, and the standard dating accuracy for zircon is about 1% (2s) accordingly. The single point ablation method was used for LA–MC–ICP–

MS laser ablation sampling, and the zircon GJ-1 was used for adjustment of the equipment so that it achieved its optimal state before data analysis. The zircon GJ-1 was taken as an external standard for zircon U-Pb dating, and the zircon M127 (U: 923 ppm; Th: 439 ppm; Th / U: 0.475. Nasdala et al., 2008) was taken as an external standard for calibration for the U, Th contents. During the test, two zircons GJ1 were measured repeatedly for calibration of samples before and after every 5–7 samples were measured. One zircon Plesovice was measured, and the equipment state should be observed to ensure the test accuracy. The ICPMSDataCal program (Liu et al. 2010) was used for data processing.  $^{206}\text{Pb}/^{204}\text{Pb} > 1000$  for vast majority of analysis points, and the common Pb correction was not performed during the test.  $^{204}\text{Pb}$  was detected by an ion counter. The analysis points with abnormally high content of  $^{204}\text{Pb}$  might be affected by the common Pb in inclusions, etc., so the analysis points with abnormally high content of  $^{204}\text{Pb}$  were excluded from the calculation. The zircon age concordia diagram was obtained with Isoplot 3.0 program. The U-Pb geochronology analysis was completed for 7 zircon samples.

Sample 0412 is quartz andesite, collected from the western Qinling orogenic belt. The zircons are euhedral and long columnar with clear edges and corners, with grain sizes being between 100–250  $\mu\text{m}$  and with length-width ratios being 2:1 generally and reaching 3:1 occasionally. Both CL and BSE images of the zircons show that the zircons have no evident cores, and are relatively clean and substantially free of inclusion, with distinct rhythmic zonal structure (Fig. 4a). The core zone density is low, but the edge zone density is higher, so the zircons are magmatic zircons.

Sample ZHZ08 is a granodiorite, collected from the western Qinling orogenic belt. The zircons are euhedral and columnar with clear edges and corners, with grain sizes being between 100–250  $\mu\text{m}$  and with length-width ratios being generally 2:1–3:1. Both CL and BSE images of the zircons show that they have no evident cores and are relatively clean, and several of them have inclusions, with weakened rhythmic zoning structure (Fig. 4). The zircons are magmatic zircons, but they might have been affected by late thermal events.

Sample ZHZ09 is an andesite, collected from the western Qinling orogenic belt. The zircons are euhedral-subhedral, and most of them are long cylindrical and several are perfectly round. The grain sizes are between 50–200  $\mu\text{m}$ , and the length-width ratios are generally 2:1–3:1. Both CL and BSE images of the zircons show that they have no nucleus and are relatively clean, and several of them have inclusions, with weakened rhythmic zoning structure (Fig. 4c). Some zircons have edges containing high U and Th and showing rhythmic zoning structure with dark luminescence, which are, however, in the same period with the core zircons. This may have been caused by the changes in the contents of U and Th in the growth of the zircon during the contemporaneous event.

Sample 0419 is a k-feldspar granite, collected from Jishishan Hill. The zircons are euhedral-subhedral, and long columnar, with grain sizes being between 100–200  $\mu\text{m}$  and with length-width ratios being generally 2:1 and occasionally reaching 4:1. Both CL and BSE images of the zircons show that they have a core-mantle-edge structure, including a white fuzzy zoning core, a gray weak zoning mantle and a black weak luminescence edge. Several zircons contain inclusions in their mantles (Fig. 4d).

Sample 0429B is a diorite, collected from Tangwang Town on the north of the Linxia basin. The zircons are subhedral-anhedral, and columnar, perfectly round, with grain

sizes being between 50–150 mm, and with length-width ratios being mostly 2:1 and 1:1 rarely. Both CL and BSE images show that the zircons have a core–mantle–edge structure, including a weakly oscillating zoning core, a gray unzoned mantle and a white narrow edge (Fig. 4e).

Sample 0429C is a k-feldspar granite, also collected from Tangwang Town. The zircons are euhedral, and long columnar, with grain sizes being between 100–150 mm and with length-width ratios being generally 2:1. Both CL and BSE images of the zircons show that they have a core–edge structure, including a white core containing inclusions, and an edge with distinct oscillating zone (Fig. 4f).

Sample 0430-2 is a granite, collected from a place about 3 km from the north of Linxia city. The zircons are euhedral and columnar, with grain sizes being between 150–200 mm, and with length–width ratios being 2:1. Both CL and BSE images show that the zircons have a homogeneous distinct oscillating zoning structure (Fig. 3g).

### 3.2.2 Analysis methods for major elements and trace elements

In order to determine the geochemical characteristics of the sample rocks, the

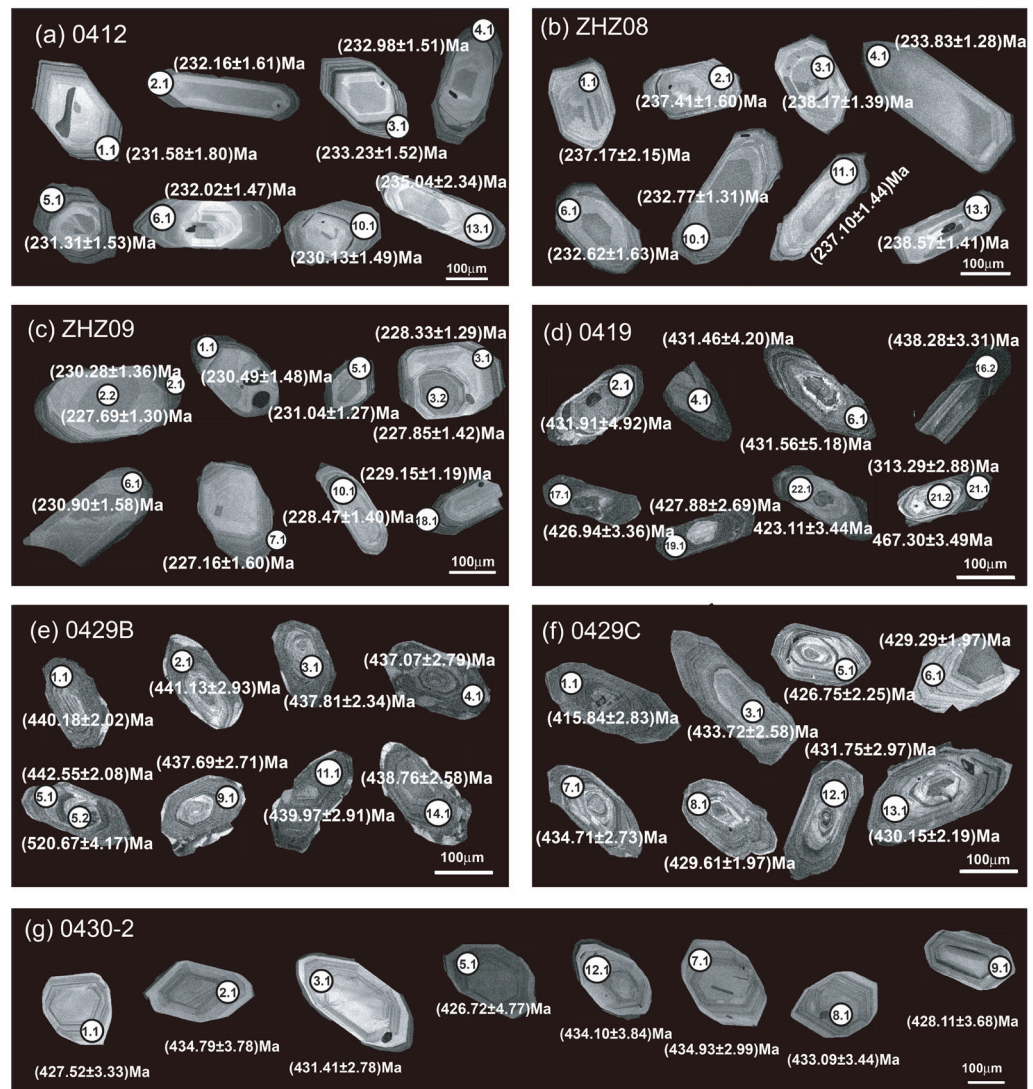


Fig. 4 CL images of representative zircons for magmatic rocks

compositions of the whole rock major elements, trace elements and Rb–Sr, Sm–Nd isotopes were analyzed. The testing of the major and trace elements was conducted at the National Geological Experiment and Testing Center of the Ministry of Land and Resources. The whole rock major elements were analyzed using the X-ray fluorescence spectroscopy (XRF) melting glass plate method. The procedure was as follows: first, put the whole rock powder into an oven to bake at 105°C for 2 hours so as to remove the adsorbed water from the sample. Remove the sample from the oven and quickly put it into a desiccator to cool. After the sample is cooled to room temperature, accurately weigh 0.5 g ( $0.5000 \pm 0.0007$ g) of the sample into a crucible dried to a constant weight, and then put the crucible with the sample into a muffle furnace and heat to 1000°C to burn for 1.5 hours. Take out the burned sample and put it in a desiccator to cool to room temperature, and then weigh it and calculate the loss on ignition of the sample. After that, accurately weigh 5 g of mixture reagent (composed of solvent  $\text{Li}_2\text{B}_4\text{O}_7$ , cosolvent LiF, oxidant  $\text{NH}_4\text{NO}_3$ ), mix with the sample, and grind till even. Pour the mixed sample into a platinum crucible, and add 3 drops of lithium bromide (release agent); pour it out after being sufficiently melted at 1000°C in the high frequency melting machine, and cool down to form a glass plate. Finally, the major element analysis of the sample was carried out by using XRF (X-ray fluorescence spectrometer 3080E). In the process of analysis, the rock standard samples GSR.1 (granite), GSR.2 (andesite) and GSR.3 (basalt) provided by the National Standard Material Center were selected as standard reference materials. In the analysis results, the analysis accuracy is 5%.

For analysis of the whole rock trace elements, the mixed acid dissolution method was used for sample dissolving. The analytical test was performed with an inductively coupled plasma mass spectrometer (ICP–MS–Excell). The analysis flow was as follows: first, put the sample into an oven to bake at 105°C for 2 hours so as to remove the adsorbed water. Take out the sample and place it in a desiccator to cool to room temperature. Weigh accurately 50.00 mg (49.00–51.00mg) of sample and put into a Teflon sample-dissolving vessel with cover, and add 1.5 mL of highly pure  $\text{HNO}_3$ , 1.5 mL of highly pure HF and 0.01 mL of highly pure  $\text{HClO}_4$ . Put the sample-dissolving vessel with cover opened on an electric heating plate at 140°C to evaporate to dryness, to remove most of the  $\text{SiO}_2$ . After drying, add 1.5 mL of highly pure  $\text{HNO}_3$  and 1.5 mL of highly pure HF again into sample-dissolving vessel. Then cover the sample-dissolving vessel, and load it into the steel jacket to seal; put into the oven at 190°C, and keep the constant temperature for 120 hours. Take out the sample-dissolving vessel, evaporate the sample to dryness, and then add 3 mL of highly pure  $\text{HNO}_3$ . Evaporate to dryness again to remove the residual HF. After that, add 3 mL of highly pure  $\text{HNO}_3$  (1:1), load into steel jacket, and put into the oven at 150°C and keep the constant temperature for 12 hours to ensure complete extraction of the sample. After cooling, pour the sample into a 100 mL PET bottle, add 1 g of Rh internal standard, and add water into the bottle to make 100 g, ready for test on the machine. The testing accuracy is 5% for trace elements and rare earth elements (REEs) with content greater than  $10 \times 10^{-6}$ , and 10% for trace elements and REEs with content less than  $10 \times 10^{-6}$ . The test error is greater than 10% for several elements with low content in the sample.

### 3.2.3 Analysis methods for whole rock Sr–Nd–Pb isotopes

The analysis of Rb–Sr and Sm–Nd isotopes was carried out at the isotope laboratory of

the Institute of Geology, Chinese Academy of Geological Sciences. First, weigh 100–150 mg of sample into a Teflon sample-dissolving vessel with cover, add 1.5 mL of highly pure HNO<sub>3</sub>, 1.5 mL of highly pure HF and 0.01 mL highly pure HClO<sub>4</sub>, and put the vessel with cover opened on an electric heating plate at 140°C to evaporate to dryness. After drying, add 1 mL of highly pure HNO<sub>3</sub> and 2 mL of highly pure HF, load into steel jacket, and put into the oven at 190°C and keep the constant temperature for 120 hours. Take out the sample and put on the electric heating plate at 140°C to evaporate to dryness. Add 1 mL of 6N HCl, evaporate to dryness again, and heat to 200°C until white smoke is fully released. Add 1 mL of 3N HCl, and keep at 80°C overnight, waiting for chemical separation. With the isotope dilution method, the composition of Sr isotopes and the concentrations of Rb, Sr, Sm and Nd were measured using Finnigan MAT-262 mass spectrometer. Nd isotope analysis was conducted using Nu Plasam HR MC-ICP-MS Multi-collector plasma mass spectrometer (Nu Instruments). The analysis results of Nd and Sr were normalized to  $^{146}\text{Nd}/^{142}\text{Nd} = 0.7219$  and  $^{86}\text{Sr}/^{88}\text{Sr} = 0.1194$ , respectively, for mass fractionation correction. During the analysis of the samples, the Sr isotope test standard was NBS987 and the test value was  $0.710247 \pm 12(2\sigma)$ . The Nd isotope test standard was JMC Nd, and the test value was  $0.511127 \pm 12(2\sigma)$ . The test accuracies of Sr and Nd isotopes are 0.000010 ( $n = 18$ ) and 0.000011 ( $n = 18$ ), respectively.

#### 4 Description of data samples

With the test data of the quartz andesite sample 0412 as an example, the composition and structure of this dataset are described.

The zircon LC-MC-ICP-MS age data of the magmatic rocks in the western Qinling orogenic belt and the Linxia basin shows the zircon U-Pb ages of the magmatic rock samples “Pb”, “Th” and “U” are the contents of three elements at test points, in  $\mu\text{g/g}$ ; “Th/U” is the content ratio of these two elements; “ $^{207}\text{Pb}/^{206}\text{Pb}(\text{Ratio})$ ”, “ $^{207}\text{Pb}/^{206}\text{Pb}(\pm\%)$ ”, “ $^{207}\text{Pb}/^{235}\text{U}(\text{Ratio})$ ”, “ $^{207}\text{Pb}/^{235}\text{U}(\pm\%)$ ”, “ $^{206}\text{Pb}/^{238}\text{U}(\text{Ratio})$ ” and “ $^{206}\text{Pb}/^{238}\text{U}(\pm\%)$ ” are corresponding isotope ratios and their errors, respectively; “ $^{207}\text{Pb}/^{206}\text{Pb}$  Age (Ma)”, “ $^{206}\text{Pb}/^{238}\text{U}$  Age (Ma)” and “Concordance” are age values and errors obtained by calculation, respectively, and the value of “ $^{206}\text{Pb}/^{238}\text{U}(\text{Ma})$ ” is used for determination of the zircon age of samples. All of the above data are measured or calculated by laboratories.

The characteristics of major elements and trace elements in magmatic rocks collected from the western Qinling orogenic belt and Linxia basin in the northern part of Hezuo show the contents of various major elements (in wt.%) and trace elements ( $\times 10^{-6}$ ) measured by laboratories; “Total”, “FeO<sup>#</sup>”, “Mg<sup>#</sup>”, “A/CNK”, “ $\Sigma\text{REE}$ ”, “Eu/Eu\*”, “Ce/Ce\*”, “(La/Yb)<sub>N</sub>”, “(La/Gd)<sub>N</sub>”, “(Gd/Yb)<sub>N</sub>” (normalized values according to Sun and McDonough, 1989), “Nb/Ta”, “Zr/Y”, “Zr/Hf”, “Rb/Sr” and “Rb/Cs” are obtained by calculation.

The characteristics of Sr and Nd isotopes in magmatic rocks collected from the western Qinling orogenic belt and Linxia basin in the northern part of Hezuo shows that “Rb( $\times 10^{-6}$ )”, “Sr( $\times 10^{-6}$ )”, “ $^{87}\text{Rb}/^{86}\text{Sr}$ ”, “ $^{87}\text{Sr}/^{86}\text{Sr}$ ” and “ $\pm 2\sigma$ ” are the contents of Rb and Sr, and the isotope ratios and errors, respectively, determined and provided by laboratories; “Sm( $\times 10^{-6}$ )”, “Nd( $\times 10^{-6}$ )”, “ $^{147}\text{Sm}/^{144}\text{Nd}$ ”, “ $^{143}\text{Nd}/^{144}\text{Nd}$ ” and “ $\pm 2\sigma$ ” are the contents of Sm and Nd, and the isotope ratios and errors, respectively, determined and provided by laboratories; “( $^{87}\text{Sr}/^{86}\text{Sr}$ )<sub>i</sub>” is the initial isotope ratio of a rock sample obtained by calculation, and “ $\epsilon_{\text{Nd}(t)}$ ” is obtained by calculation.

## 5 Data usage

The above test result data are provided by known laboratories. With zircon U–Pb age data, the zircon age concordia diagram can be obtained using the program Isoplot 3.0. The test data of major elements, trace elements and rock Sr–Nd can be used respectively for geochemical mapping to obtain the geochemical characteristics of rock, and then to infer the formation mechanism of rock samples and the tectonic setting of the research area.

## 6 Conclusions

The geochemical dataset of important magmatic rocks along the deep seismic reflection profile of the western Qinling—Linxia basin comprises three data sheets, namely, the zircon LA - MC - ICP - MS age data for magmatic rocks in the western Qinling orogenic belt and Linxia basin (a total of 7 test samples, 145 test points), the characteristics of major elements and trace elements of the magmatic rocks in the northern part of Hezuo (a total of 33 test samples, with 69 test items per sample), and the characteristics of Sr and Nd isotopes of the magmatic rocks (a total of 27 test samples). These data from the western Qinling orogenic belt and Linxia basin provide scientific reference for the study of the lithogenesis and geological and tectonic setting in the area.

## References

- Fang Xiaomin, Li Jijun, Zhu Junjie, Chen Huailu, Cao Jixiu. 1997. Absolute age determination and division of Cenozoic strata in Linxia basin, Gansu Province [J]. *Chinese Science Bulletin*, 42(14): 1457–1471 (in Chinese).
- The Field Team of Gansu Province. 1965. 1:200000 Map of the Geological Map of the People's Republic of China, Linxia [M]. Beijing: Geological Publishing House (in Chinese).
- Li Jijun, Fang Xiaomin, Zhu Junjie. 1995. Paleomagnetism and patterns of Cenozoic strata in Linxia basin [C]//Formation and Evolution of the Qinghai - Tibet Plateau, Environmental Change and Ecosystem Research (1994). Beijing: Science Press, 41–54 (in Chinese).
- Sun S S, McDonough W F. 1989. Chemical and Isotopic Systematics of Oceanic Basalts: Implications for Mantle Composition and Processes [M]. Geological Society, London, Special Publications, 42: 313–34.
- Yu Xuehui, Mo Xuanxue, Martin F, Su Shangguo, Zhao Xin. 2001. Cenozoic kamafugite volcanism and tectonic meaning in west Qinling area, Gansu province [J]. *Acta Petrologica Sinica*, 17(3): 366–377 (in Chinese with English abstract).
- Yu Xuehui. 1994. Cenozoic potassic alkaline ultrabasic volcanic rocks and its genesis in Lixian—Dangchang area, Gansu Province [J]. *Tethyan Geology*, 18: 114–129 (in Chinese).
- Zheng Dewen, Zhang Peizhen, Wan Jinglin, Li Chuanyou, Cao Jixiu. 2003. Timing of Late Cenozoic tectonic deformation in the northeastern margin of the Qinghai-Tibet Plateau - Apricot fission track record of detrital particles in Linxia basin [J]. *Science in China (Series D)*, 33(sup.): 190–198 (in Chinese).